Polar lattice dynamics of the $MgAl_2O_4$ spinel up to the liquid state

2006 J. Phys.: Condens. Matter 18 5669

(http://iopscience.iop.org/0953-8984/18/24/008)

INSTITUTE OF PHYSICS PUBLISHING JOURNAL OF PHYSICS: CONDENSED MATTER

J. Phys.: Condens. Matter **18** (2006) 5669–5686 doi:10.1088/0953-8984/18/24/008

Polar lattice dynamics of the $MgAl_2O_4$ spinel up to the liquid state

D De Sousa Meneses[1,2], **J-F Brun**[1], **B Rousseau**[1] **and P Echegut**[1]

[1] CNRS-CRMHT, 1D Avenue de la Recherche Scientifique, 45071-Orléans cedex 2, France
[2] Polytech Orléans, 8, rue Léonard de Vinci, 45072-Orléans cedex 2, France

E-mail: desousa@cnrs-orleans.fr

Received 6 February 2006
Published 2 June 2006
Online at stacks.iop.org/JPhysCM/18/5669

Abstract

Emittance spectra of the $MgAl_2O_4$ spinel have been obtained up to 2500 K. Spectral analysis using a dielectric function model recently developed for amorphous materials allowed us to retrieve the inversion parameter over a very wide temperature range. The results are very close to the most recent published values. Both the Landau and the O'Neill and Navrotsky thermodynamic models allow a satisfactory fit to the experimental data. In the mid-infrared range, a sudden increase of the emittance appears more than 200 degrees below the solid to liquid transition. The mechanism of absorption is very well described by a Debye process for which both dielectric contribution and relaxation time are thermally activated. Finally, we showed that the change of phase leads to an abrupt modification of the lattice dynamics and that change evolves rapidly in the liquid state.

1. Introduction

Spinel has received considerable attention because of its excellent physicochemical properties that make it suitable for various industrial applications [1–3] and its scientific interest both in material and earth sciences. The general formula of spinel is $(A_{1-x}B_x)[A_xB_{2-x}]O_4$, where parentheses stand for tetrahedral sites and the square brackets for octahedral ones. x represents the inversion parameter. In 2–3 spinels, its value can vary between 0 for *normal* spinel to 1 for the *inverse* spinel and corresponds to the fraction of trivalent B cations that occupy tetrahedral sites. The order–disorder in spinel is of the non-convergent type which implies that the symmetry of the compound remains the same whatever the value of the inversion parameter. Even if the goal of a lot of experimental [4–12] and theoretical [13–16] works was the determination of the inversion parameter, both its absolute value and temperature dependence are still controversial because of the large spread of the published data. A precise determination of this parameter within the largest range of temperature is then always topical and necessary for a correct evaluation of the different thermodynamic description of $MgAl_2O_4$.

Disorder also has a deep impact on the lattice dynamics of the spinel, as shown by infrared spectroscopy [17–23], Raman [24, 25] spectroscopy and first-principles calculations [26, 27]. As far as we know, only Raman studies [24, 25] have investigated the temperature behaviour of phonon modes and only in a limited range of temperature, below 1273 K.

In this paper, we report the normal spectral emittance of magnesium spinel up to the liquid state. A careful analysis of the experimental spectra with an adequate dielectric function model allowed us to retrieve the relative temperature dependence of the inversion parameter over a very wide range. More than 200 degrees below the melting point, the transparency in the mid-infrared range of the spinel disappears progressively due to a thermally activated absorption mechanism which is well described by a Debye relaxation. Finally, a discussion about the solid to liquid phase will be given in the light of the evolution of the lattice dynamics.

2. Experimental procedure

All the results presented hereafter have been obtained on Czochralski-grown synthetic $MgAl_2O_4$ spinel provided by the MTI Corporation. The samples are plates oriented perpendicularly to $\langle 100 \rangle$, optically polished and with the following dimensions: $(5 \times 5 \times 0.5)$ mm^3. A first set of measurements has been made to determine the normal spectral emittance of the material from room temperature up to 2300 K (figure 1) and a second set reported in a following section was obtained in a restricted spectral range (400–5000 cm^{-1}) and focused more on the solid to liquid phase transition. The data acquisition has been performed with an enhanced Bruker IFS 113 v spectrometer that has been described in a previous work [28]. The room temperature normal spectral emittance E was obtained from the reflectance R and transmittance T spectra obtained at normal incidence and by applying Kirchhoff's law and energy balance:

$$E = 1 - R - T. \tag{1}$$

This procedure is often called the indirect method of determination of the emittance [28]. The other spectra were obtained by the direct method, which consists of comparing the flux emitted by the sample to the one of a black body reference. In practice the following protocol, which we name the three interferograms method, is used. Why are three interferograms measured? Because the surroundings and the spectrometer itself are at room temperature which implies that the flux S measured by the detector does not come solely from the focus point of the optical system where the sample is placed but also from the surroundings. If one assumes that the surrounding radiation near the focal point is a black body one at a temperature θ_S, the different sources contribute to the measured signal in the following way:

$$S(\theta_{Obj}, \theta_S) = S_p + f[E(\theta_{Obj})L(\theta_{Obj}) + R(\theta_{Obj})L(\theta_S) + T(\theta_{Obj})L(\theta_S)], \tag{2}$$

where S_p stands for all the parasitic fluxes that do not come from the focal point, f is an extended transfer function that takes into account the geometry of the optical path (solid angle, aperture, magnification, ...) and the losses occurring between the focal point and the detector, L is the Planck function and θ_{Obj} is the temperature of the object situated at the focal point of the optical system. Introducing equation (1) gives for equation (2):

$$S(\theta_{Obj}, \theta_S) = S_p + f[E(\theta_{Obj})(L(\theta_{Obj}) - L(\theta_S)) + L(\theta_S)]. \tag{3}$$

The relation can be further simplified in the case where the object situated at the focal point is a black body reference. So $E(\theta_{BB}) = 1$ and S becomes:

$$S_{BB}(\theta_{BB}, \theta_S) = S_p + fL(\theta_{BB}). \tag{4}$$

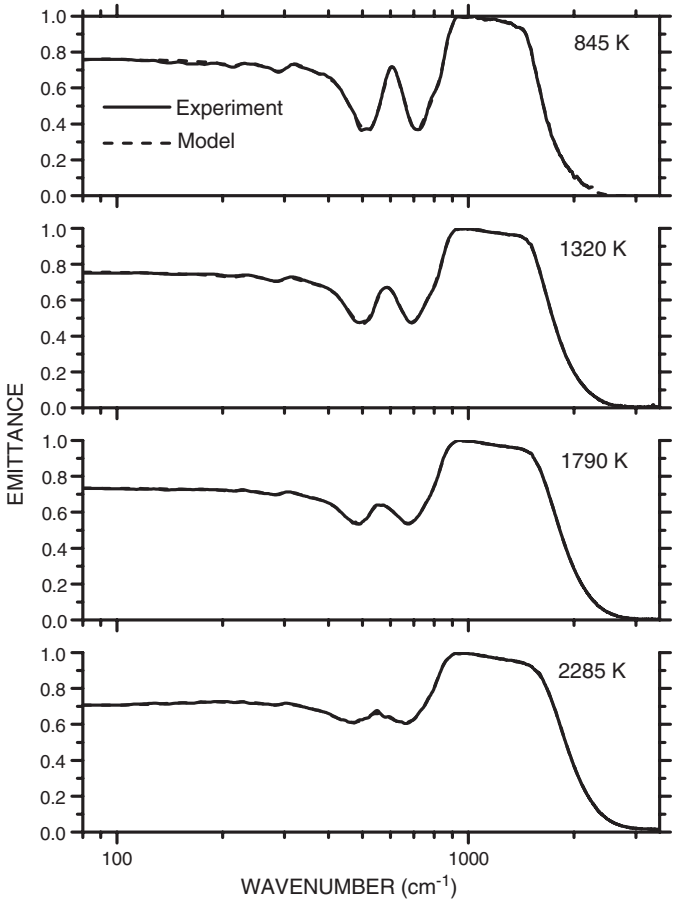

Figure 1. Temperature dependence of the normal spectral emittance of the $MgAl_2O_4$ spinel. Solid lines represent the experimental data and dashed lines the best fits using equation (15).

The following case $\theta_{Obj} = \theta_S$, that means temperature of the object is equal to the surrounding radiation temperature, gives a second simplification:

$$S_S(\theta_S) = S_p + fL(\theta_S). \tag{5}$$

Equations (3)–(5) constitute the base of the three interferograms method. A first interferogram I_S is recorded with the conditions of equation (5). The second one I_{BB} is measured from a black body reference and the latter I, corresponding to equation (3), is obtained with the sample exactly placed at the focus point.

Knowledge of these three interferograms acquired with identical temperatures for the black body reference and the sample is sufficient to determinate the emittance of the sample:

$$E(\theta_{Obj}) = \frac{FT(I - I_S)}{FT(I_{BB} - I_S)}, \tag{6}$$

where FT designates the Fourier transform.

Equation (6) is well defined if the temperature T is well fixed and accurately measured. These conditions are not easily verified for the extreme temperatures investigated in this work. In the case of polar dielectric materials like spinel, there is a particular wavenumber, called

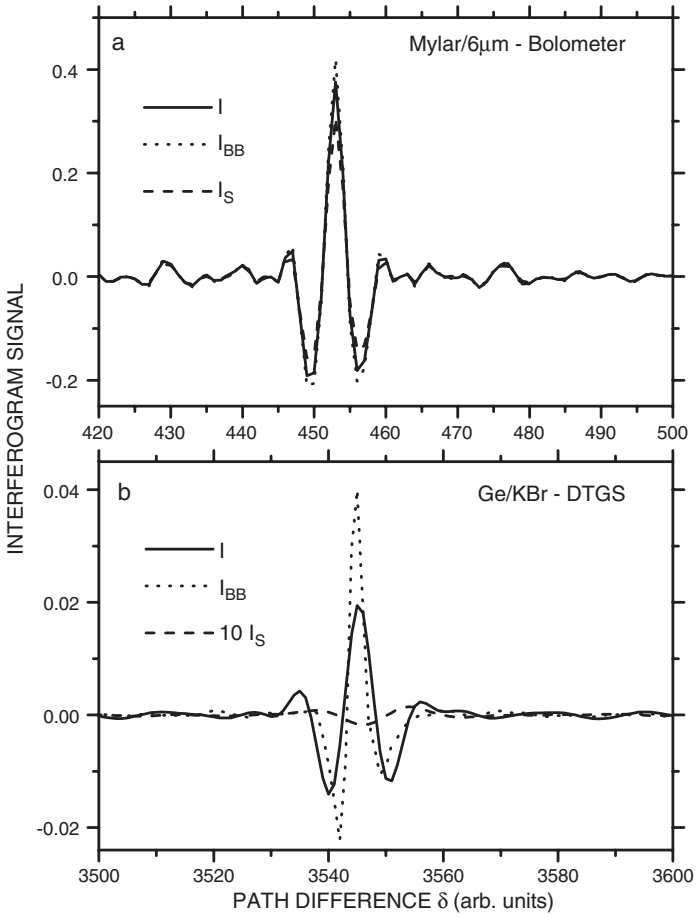

Figure 2. Example of a set of three interferogram signals used in the determination of an emittance spectrum. See text for more details.

the Christiansen point, for which the material behaves nearly like a black body whatever its temperature. This peculiar property is useful for performing accurate measurement of the sample temperature by using the spectrometer as a pyrometer working at the Christiansen point, i.e. at around 980 cm^{-1} in the case of $MgAl_2O_4$. For stability reasons and because we are sure that the detectors in our setup are linear for the conditions of measurement, the black body furnace is maintained at the same temperature of around 1700 K for every measurement. Within these conditions, the emittance of the sample is obtained by applying:

$$E(\theta_{\mathrm{Obj}}) = \frac{\mathrm{FT}(I - I_{\mathrm{S}})}{\mathrm{FT}(I_{\mathrm{BB}} - I_{\mathrm{S}})} \frac{L(\theta_{\mathrm{BB}}) - L(\theta_{\mathrm{S}})}{L(\theta_{\mathrm{Obj}}) - L(\theta_{\mathrm{S}})}. \tag{7}$$

Figure 2 presents a three interferogram set. In the spectral range 80–500 cm^{-1} the measurements were made with a bolometer and a mylar (6 μm) beam splitter. Between 400 and 5500 cm^{-1} a deuterated triglycine sulfate (DTGS) detector and a Ge/KBr beam splitter were used. An experimental resolution of 4 cm^{-1} was chosen for every measurement. A 250 W CO_2 laser was used to heat the sample. This type of heating has several advantages. First it allows efficient heating up to 2500 K. The energy is locally deposited; this fulfils the assumption of room temperature for the surroundings. Finally it allows the liquid state to be reached by

applying the autocrucible technique. In the latter method only the centre of the sample is heated; the border, still in the solid state due to the thermal gradient, acts as a crucible for the liquid phase. To make accurate measurements, the spectrometer is focused on a small isothermal liquid spot of the sample thanks to an aperture placed at a focal point of the optical system. For one of the samples, a temperature of about 2530 K was been reached which represents more than 100 degrees in the liquid state. For the low temperature measurements, typically below 1000 K, the signal to noise ratio unsatisfactorily decreases because of the weakness of the acquired fluxes. These measurements are nevertheless reported in this paper because they give reasonable results.

3. Spectral analysis

Emittance is directly related to reflectance and transmittance (see equation (1), Kirchhoff's law). So dielectric function models, well known to retrieve the optical functions of a material, can be extrapolated to fit the normal spectral emittance. In the opaque zone, for which $E = 1 - R$, the reflectivity models can be directly applied. In the case of $MgAl_2O_4$, two types of dielectric function models have been used in the literature: the classical Lorentz oscillator model [19, 20, 22] and the generalized Lyddane–Sachs–Teller relationship [23]. Even though previous models have been successfully used to retrieve the optical functions in the phonon zone at room temperature, they are not used in the present work. Indeed, it was clearly shown [29] that these expressions are inadequate for reproducing the optical response of multi-phonon processes in the semi-transparent spectral range of crystals. Then a complete analysis of the acquired spectra is not possible within this framework. Besides, fits with both good quality and physical meaning are not easily reachable from experimental spectra in the phonon zone and above 1200 K. In the light of these first results, another model, based on a causal version of the Voigt function, was developed [30]. This model, whose particularity is to be able to reproduce absorption profiles that change from Lorentzian to Gaussian, has been used successfully. The results indicated unambiguously that the absorption profiles of the vibrations are mainly of Lorentzian character at room temperature, change progressively towards the Gaussian shape upon increasing temperature and become essentially Gaussians above 1200 K. In this work, we focus on the high temperature properties, so only results obtained with a simplified version of this dielectric function are reported. The model, based on causal Gaussian absorption profiles, allows us to reproduce the experimental data in the whole spectral range with a reduced set of parameters, as can be seen in the figures to follow.

The classical Gaussian function g is given by:

$$g(\omega; A, \omega_0, \sigma) = A \exp\left(-4 \ln 2 \left(\frac{\omega - \omega_0}{\sigma}\right)^2\right), \tag{8}$$

where A, ω_0 and σ represent the amplitude, the peak position and the full width at half maximum, respectively. This function cannot be used as it is to describe an absorption peak because the expression is not causal. A causal version g_c can be easily obtained by applying the following relation:

$$g_c(\omega; A, \omega_0, \sigma) = g(\omega; A, \omega_0, \sigma) - g(\omega; A, -\omega_0, \sigma). \tag{9}$$

The real part of the dielectric function g_c^{kkg} corresponding to g_c is obtained by using the adequate Kramers–Kronig relation:

$$g_c^{kkg}(\omega; A, \omega_0, \sigma) = \frac{2A}{\sqrt{\pi}} \left[D\left(2\sqrt{\ln 2}\frac{\omega + \omega_0}{\sigma}\right) - D\left(2\sqrt{\ln 2}\frac{\omega - \omega_0}{\sigma}\right)\right]. \tag{10}$$

D stands for the Dawson function:

$$D(x) = \exp(-x^2) \int_0^x \exp(t^2)\, \mathrm{d}t. \tag{11}$$

for which efficient numerical algorithms exist. The area a_{gc} under the g_c curve is also given by another special function:

$$a_{gc} = \int_0^\infty g_c(\omega)\, \mathrm{d}\omega = \frac{\sigma}{2}\sqrt{\frac{\pi}{\ln 2}}\, \mathrm{erf}\left(2\sqrt{\ln 2}\frac{\omega_0}{\sigma}\right), \tag{12}$$

where erf is the error function:

$$\mathrm{erf}(x) = \frac{2}{\sqrt{\pi}} \int_0^x \exp(-t^2)\, \mathrm{d}t. \tag{13}$$

The position of the maximum $\omega_{\max}$ of the causal Gaussian g_c can be computed by using the following numerical sequence:

$$\begin{aligned} \omega_{\max} &= \lim_{n\to\infty} \omega_n \\ \omega_{n+1} &= (\omega_n + \omega_0) \exp\left(-16 \ln 2 \frac{\omega_n \omega_0}{\sigma^2}\right) + \omega_0, \end{aligned} \tag{14}$$

to the wanted precision.

The above results represent one of the building blocks of the dielectric function model ε used in this work:

$$\varepsilon(\omega) = \varepsilon'(\omega) + \mathrm{i}\varepsilon''(\omega) = \varepsilon_\infty + \sum_j (g_{cj}^{\mathrm{kkg}}(\omega) + \mathrm{i}g_{cj}(\omega)) + \frac{\Delta}{1 - \mathrm{i}\omega\tau} = \varepsilon_\infty + \sum_j \tilde{g}_{cj}(\omega) + \frac{\Delta}{1 - \mathrm{i}\omega\tau}. \tag{15}$$

ε_∞ is the high frequency dielectric constant that takes into account the electronic contribution; the sum term is able to reproduce both phonon modes and multi-phonon contributions and in the last term Δ and τ represent respectively the dielectric strength and the characteristic time of a Debye relaxation. The latter term is only used to fit the spectra at temperatures above 2000 K for which another absorption mechanism appears in the transparent region. All the fits reported in this paper have been performed with FOCUS [31].

In figure 3, the model was used to reproduce the reflectance, the transmittance and the emittance spectra of $MgAl_2O_4$ obtained at room temperature with a single set of parameters. As can be seen in this figure, good agreement is obtained in the whole spectral range even if, and as previously quoted, this model is not the most adequate at room temperature. To reproduce all the features appearing in the room temperature spectra, it was necessary to introduce nine Gaussians within the phonon region and another five Gaussians to take into account the multi-phonon processes in the semi-transparent zones. The parameter values are reported in table 1.

$MgAl_2O_4$ exhibits a cubic structure with space group $Fd3m(\mathrm{O}_\mathrm{h}^7)$. The symmetry analysis shows that in addition to the three acoustic modes, there are 39 optic modes distributed among the following symmetries at the Γ point:

$$\mathrm{A_{1g}(R)} + \mathrm{E_g(R)} + 3\mathrm{T_{2g}(R)} + 4\mathrm{T_{1u}(IR)} + \mathrm{T_{1g}} + 2\mathrm{A_{2u}} + 2\mathrm{E_u} + 2\mathrm{T_{2u}},$$

where R and IR denote Raman or infrared activity, respectively, and the remaining modes are silent [23]. Group theory only predicts four infrared active modes for a normal $MgAl_2O_4$ spinel. Disorder can explain that we need nine phonon modes to reproduce the experimental spectra of the synthetic spinel. In order to give graphical support to our discussion, we have reported in figure 4 in a logarithmic scale the imaginary part of the dielectric function at room temperature and the individual contributions of each phonon mode. The ν_2, ν_5, ν_6 and

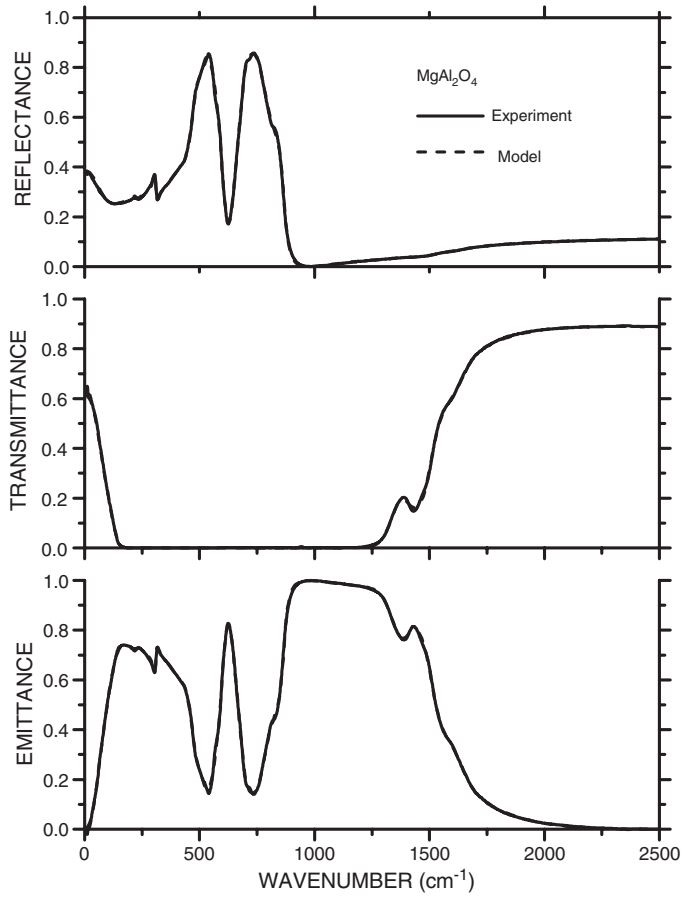

Figure 3. Room temperature reflectance, transmittance and emittance spectra of $MgAl_2O_4$ (solid lines) and best fits using equation (15) with the parameters of table 1 (dashed lines).

ν_8 modes are the symmetry allowed ones, they correspond to the D, B2, B1 and A modes, respectively, in Fabian's nomenclature. A comparison between the vibrational wavenumbers obtained in this work and results in the literature is reported in table 2. As can be seen, even if different phenomenological dielectric functions models (the Drude Lorentz model, the generalized Lyddane–Sachs–Teller relationship and the causal Gaussian model) have been used to extract frequencies from the experimental spectra a really good agreement is found for all the phonon mode frequencies. These values are also close to those obtained from first-principles calculations [23, 27]. According to Preudhomme and Tarte [18], and confirmed later by Fabian *et al* [22], the ν_2 mode must be assigned to a Mg–O vibration. The remaining three modes are all attributed to the trivalent octahedral cation, i.e. to Al–O vibrations [18, 22].

Besides the four allowed modes, there are five supplementary modes. The first one (ν_1), situated around 224 cm^{-1}, has also been observed by Thibaudeau *et al* [23]. These authors attributed its existence to the existence of disorder. Indeed, the loss of translational symmetry due to cation disorder leads to the activation of IR modes that are normally inactive. Da Rocha *et al*, from the same team, have confirmed this by using density functional perturbation theory (DFPT) to calculate infrared phonons for different amounts of disorder [13]. By comparing reflection spectra of natural and synthetic spinels, Fabian *et al* [22] have also clearly shown

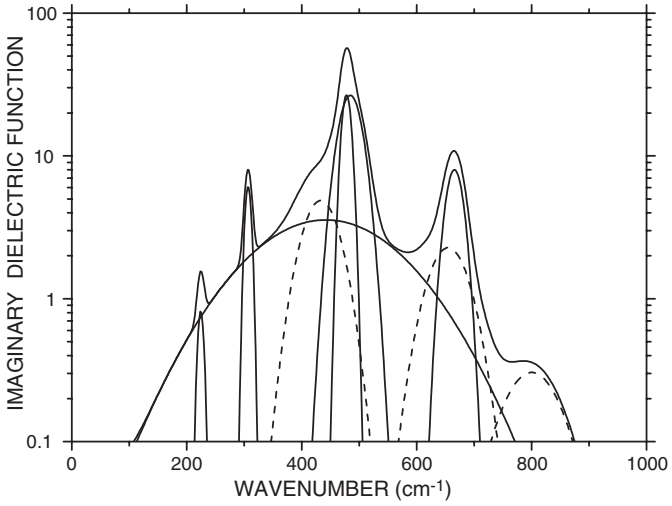

Figure 4. Phonon contributions to the imaginary part of the dielectric function. Dashed lines represent the phonon modes that have been omitted in the fits of the experimental data obtained above 700 K.

Table 1. Amplitudes (A), wavenumbers (ω_0) and full widths at half maximum (σ) of the causal Gaussian peaks. Equation (15) was used to fit the reflectance, transmittance and reflectance spectra of $MgAl_2O_4$ at room temperature. $\varepsilon_\infty = 2.9$. ν_j and m_j designates respectively phonon modes and multi-phonon contributions.

$\tilde{g}_{cj}$	A	ω_0 (cm^{-1})	σ (cm^{-1})
m_1	0.02	76.5	66.7
ν_1^a	0.82	224.3	12.4
ν_2^a	6.13	306.8	13.2
ν_3	4.87	433.1	72.9
ν_4^a	3.56	442.1	289.8
ν_5^a	26.60	477.9	19.8
ν_6^a	26.60	484.6	46.7
ν_7	2.28	654.7	81.3
ν_8^a	8.01	665.7	35.3
ν_9	0.30	800.2	112.2
m_2	0.0031	916.0	913.8
m_3	0.0300	1115.2	275.5
m_4	0.0038	1446.1	110.3
m_5	0.00063	1573.8	142.4

[a] Phonon modes used for the fits obtained above room temperature.

that cation disorder, i.e. the partial transition of Al ions to tetrahedral sites and Mg ions to octahedral sites, leads to the appearance of new modes. These modes are broad and appear in the low frequency side of the strong phonon modes. Such a result is once more confirmed by Cynn [24] and Minh [25]; their Raman spectra on natural and annealed or synthetic spinels show that the 410 cm^{-1} mode presents an obvious asymmetry. The latter assigns this evolution to the appearance of a new bending mode at 400 cm^{-1} whose origin is due to the presence of Al ions in tetrahedral sites. In the same way, the DFPT calculations of Darocha *et al* [13] show that infrared phonons are highly sensitive to the amount of disorder and that broad absorption

Table 2. Comparison between the wavenumbers of the symmetry allowed modes obtained in this work and results reported in the literature.

Reference	ν_2 (cm^{-1})	ν_5 (cm^{-1})	ν_6 (cm^{-1})	ν_8 (cm^{-1})
[32]	305	428	485	670
[22][a]	306.9	488.5	511.3	672.6
[23][a]	303	491	532	675
[23][b]	307	478	565	666
[26][b]	337	481	497	664
This work[a]	306.8	477.9	484.6	665.7

[a] Experimental vibrational wavenumbers.
[b] First-principles calculations.

is present below symmetry allowed phonon modes. The broad modes (ν_3, ν_4, ν_7 at room temperature and ν_4 at higher temperatures) introduced in our model to take account of the density of vibrational states resulting from disorder in our synthetic spinel are thus in complete agreement with the literature on the subject. If we exclude the ν_1 mode, the number of modes used in this study is also in agreement with those used by Fabian *et al* [22]. The weak mode ν_9 situated around 800 cm^{-1} has been also assigned to the defective nature of the synthetic spinel and was tentatively attributed to an Al–O vibration involving tetrahedrally coordinated Al ions [22].

Another effect of cation disorder, described by almost all of the authors, is the broadening of most of the modes [20]. The reported values are intermediate between those of crystals and glasses. This explains why a model that was initially developed to reproduce infrared spectra of amorphous compounds also fits well the emittance spectra of synthetic $MgAl_2O_4$. With increasing temperature, the broadening become so important that is no longer possible to clearly resolve all the modes. So we choose to conserve besides the strongest modes the ones appearing without any ambiguity, such as the ν_1 one. A reduced set of six phonon modes was used to fit the emittance spectra above room temperature. The omitted modes are represented in figure 4 by dashed lines.

4. Lattice vibrations versus inversion parameter

As already quoted, disorder plays a crucial role in the optical response of the $MgAl_2O_4$ spinel. Also a careful study of the infrared response up to high temperature can lead to useful information on the temperature dependence of the inversion parameter. The knowledge of this parameter for a wide range of temperature is of great interest, for instance to test the different thermodynamic approaches to cation ordering [5, 14]. Figure 1 shows characteristic fits of the normal spectral emittance of the synthetic spinel. The temperature dependence of the parameters corresponding to the lattice vibrations are also given in figures 5–7. The peak positions show a linear decrease with increasing temperature, which is the normal behaviour. The combination of the temperature effect and the increase in the inversion parameter also leads to an important broadening of the strong vibrations. Above 2000 K, it was necessary to introduce a supplementary mode (ν_{sup}) to take into account the extra absorption appearing in the far infrared range. The main result of the analysis is observable in figure 6, showing the amplitude dependence with temperature. One can observe the same general decreasing trend for most of the modes. On the contrary the ν_4 mode, which is clearly connected to disorder, exhibits the opposite behaviour. Its temperature dependence looks like the published data for the inversion parameter [4]. So a deeper analysis of the dielectric strength of this mode is

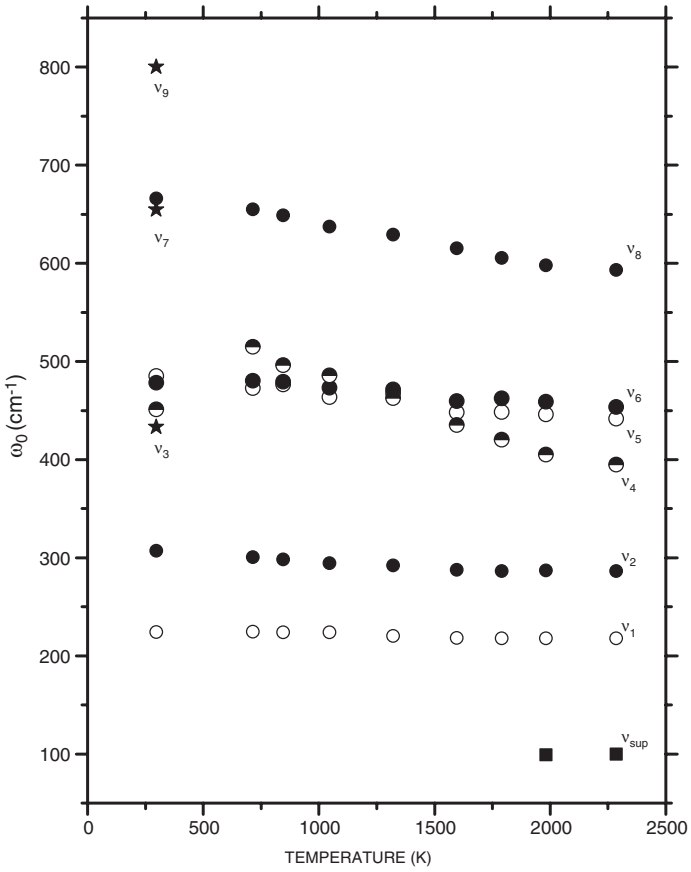

Figure 5. Temperature dependence of the position of the phonon modes of $MgAl_2O_4$. Stars represent weak phonon modes used to fit only the room temperature spectra. ν_{sup} is a supplementary mode introduced at high temperature to describe an extra absorption appearing in the far infrared range.

reported hereafter. Since the literature shows a large dispersion of the values obtained for the inversion parameter, it is not possible to compare the temperature dependence of the dielectric strength of the ν_4 mode with the published data by using simply a scaling factor. An alternative approach is proposed here, and consists of using the constraints of thermodynamic models. This method is suitable because we have obtained the dielectric strength within a very wide temperature range. Landau functions have been often used to describe phase transitions in minerals and were also used to fit the cation disorder of $MgAl_2O_4$. For this compound, a general formula for the excess free energy of ordering ΔG has been expressed as an expansion in terms of the order parameter Q [5, 14, 33, 34]:

$$\Delta G(Q;T) = -hQ + \frac{a}{2}(T - T_c)Q^2 + \frac{b}{n}Q^n, \tag{16}$$

where h, a, b and T_c are constants. n equals 4 or 6. With the condition $\partial G/\partial Q = 0$ and the constraint that the order parameter equals unity at vanishing temperature, the following expression relating Q and T is obtained:

$$T = T_c + \frac{T_c}{(p-1)Q}(1 - pQ^{n-1}), \tag{17}$$

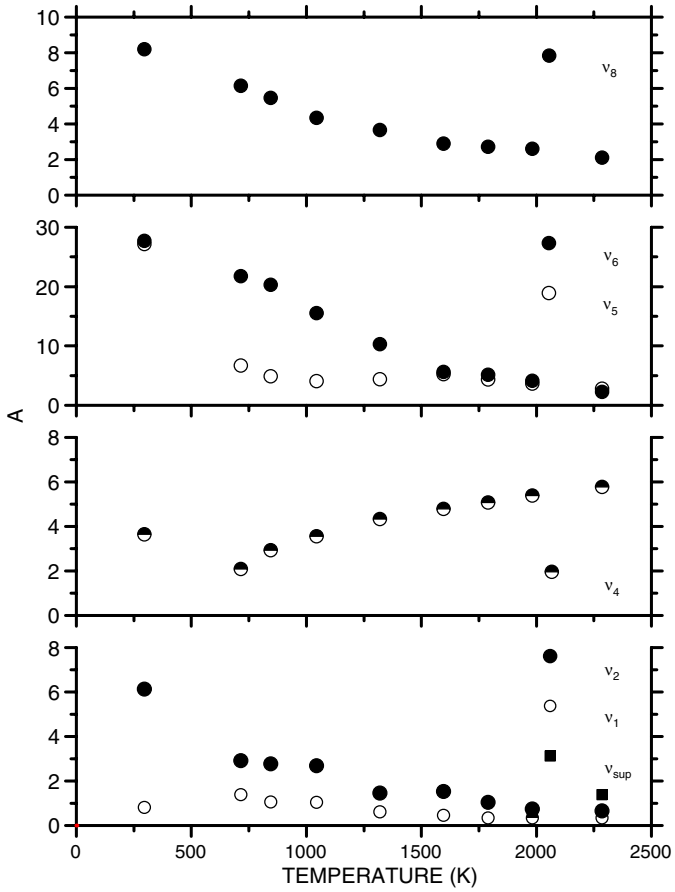

Figure 6. Temperature dependence of the amplitudes of the lattice modes of $MgAl_2O_4$.

where $p = b/h$. An exploratory analysis has shown that in our case $T_c = 0$ K. The previous model can be simplified for a vanishing T_c and equation (17), linking Q and T, becomes:

$$T = r\frac{1 - Q^{n-1}}{Q}, \tag{18}$$

where $r = b/a$.

If we express the inversion parameter $x = \frac{2}{3}(1 - Q)$ as a linear function of the area ξ of the ν_4 mode:

$$x = s\xi, \tag{19}$$

both r and s can be deduced from a least square fit of the temperature dependence of ξ using equations (18) and (19). The best fits corresponding to $n = 4$ and 6 were obtained with the following values: $r_4 = 1241$ and $r_6 = 799$ (the room temperature point was not included in the optimization process). The resultant inversion parameters $x_4 = s_4\xi$ and $x_6 = s_6\xi$ are reported in figures 8 and 9 and in table 3. As can be seen, even if the estimations are different for the two values of n, they nevertheless remain within the range of experimental results. A better fit is obtained by using the following excess free energy:

$$\Delta G(Q; T) = -hQ + \frac{a}{2}TQ^2 + \frac{b}{4}Q^4 + \frac{c}{6}Q^6, \tag{20}$$

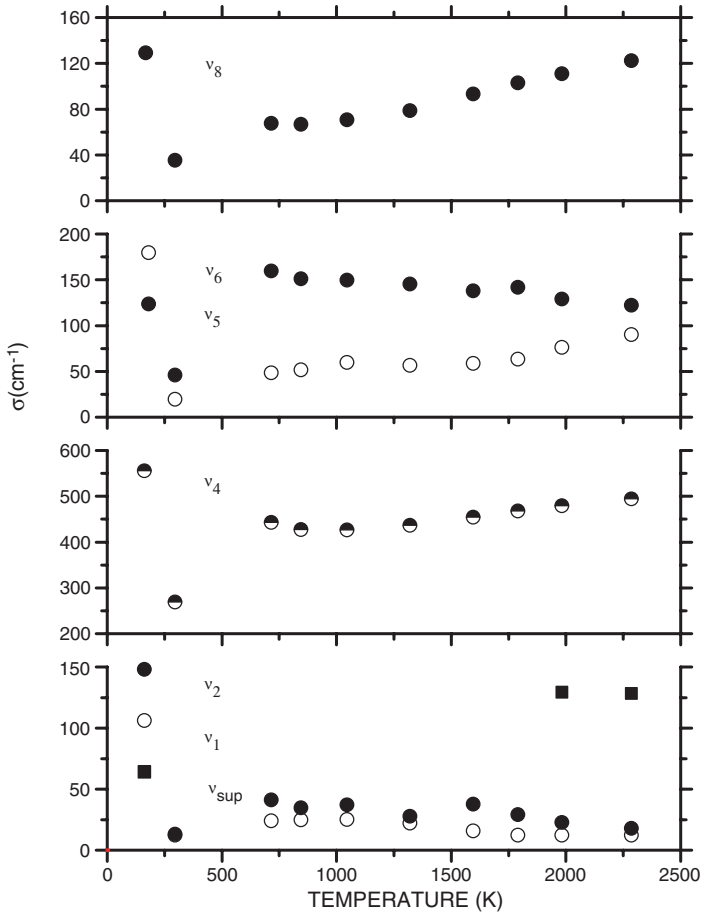

Figure 7. Temperature dependence of the full width at half maximum of the lattice modes of $MgAl_2O_4$.

Table 3. Estimations of the inversion parameter obtained by least square fitting the experimental data with different Landau models.

T (K)	x_4	x_6	$x_{4\&6}$
296	0.119	0.151	**0.134**
715	0.111	0.142	**0.126**
845	0.151	0.192	**0.170**
1045	0.184	0.234	**0.207**
1320	0.229	0.291	**0.258**
1596	0.263	0.335	**0.297**
1790	0.287	0.365	**0.323**
1982	0.313	0.398	**0.353**
2285	0.345	0.439	**0.389**

and the associated relation:

$$T = -\frac{u + vQ^3 - (u - v)Q^5}{Q}, \tag{21}$$

where $u = h/a$ and $v = b/a$.

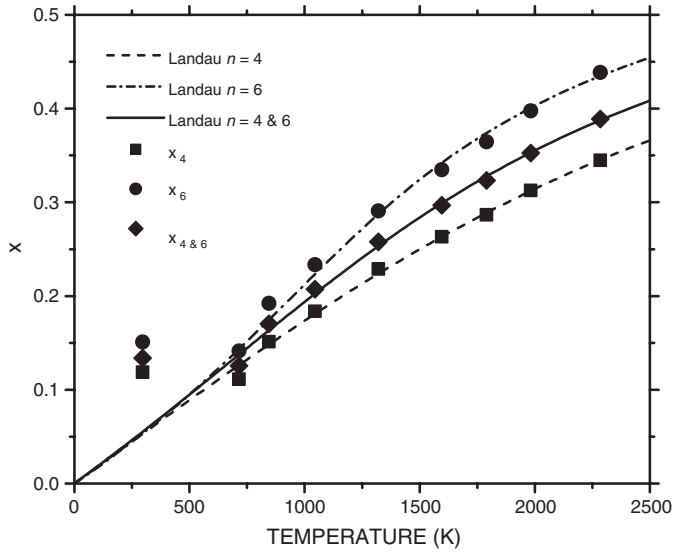

Figure 8. Estimations of the inversion parameter x obtained with least square regressions based on different Landau functions (lines). Squares, circles and diamonds represent the renormalizations of the experimental data ξ with the scaling factors s_4, s_6 and $s_{4\&6}$, respectively. See text for more details.

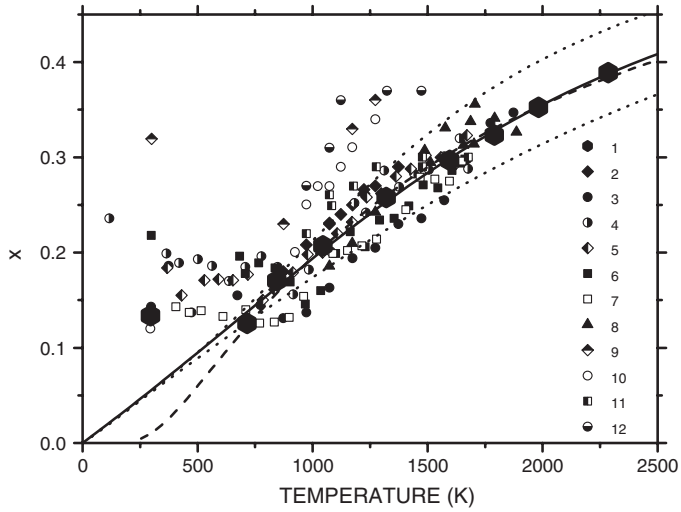

Figure 9. Comparison between the temperature dependence of the inversion parameter obtained in this work and various sets reported in the literature: (1) this work, (2) Andreozzi *et al* [4] (3)–(7) Redfern *et al* [5], respectively heating data from ISIS, heating and cooling of $Mg_{0.99}Al_2O_4$, heating and cooling data from IPNS, (8) Maekawa *et al* [7] (9), (10) Peterson *et al* [9], (11) Millard *et al* [8], (12) Wood *et al* [10]. The solid line represents the best fit with the 4&6 Landau model. Dotted lines represent fits with Landau model 4 and Landau model 6. The dashed curve is the best fit with the O'Neill and Navrotsky thermodynamic model.

The new adjustment of the experimental data is characterized by $\chi^2_{4\&6}/\chi^2_4$ and $\chi^2_{4\&6}/\chi^2_6$ ratios that evaluate respectively to 0.8 and 0.5 and lead to an inversion parameter $x_{4\&6} = s_{4\&6}\xi$ that lies between those obtained with the previous fits (figure 8). The resulting values are

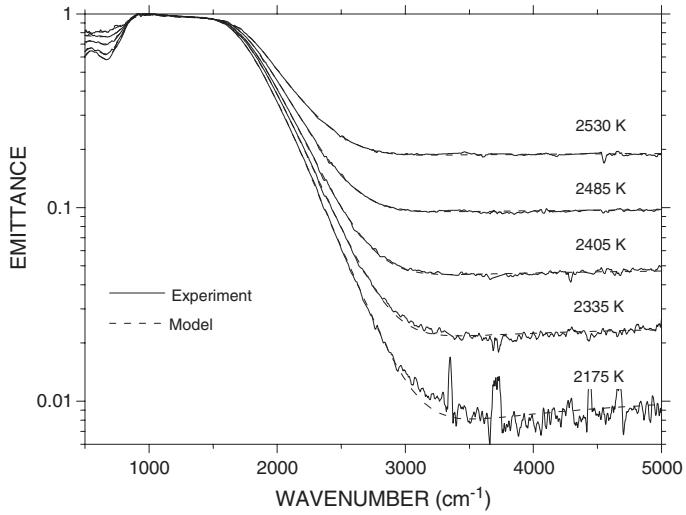

Figure 10. Set of emittance spectra of $MgAl_2O_4$ in both solid and liquid states. Dashed lines represent the best fits of the experimental spectra with equation (15).

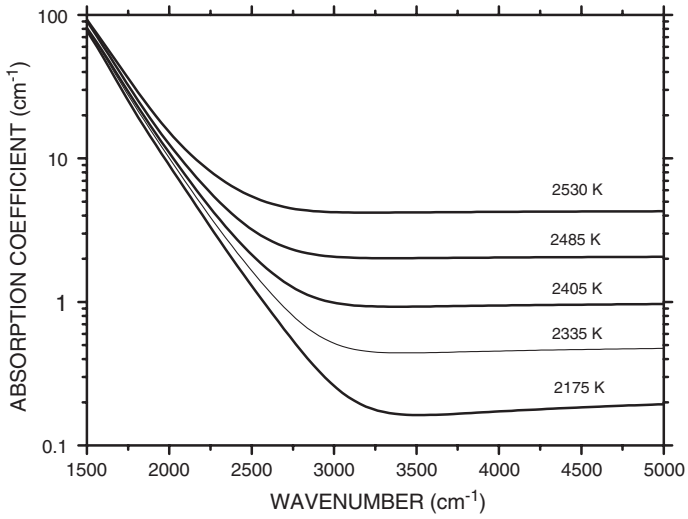

Figure 11. Temperature dependence of the absorption coefficient in the mid-infrared range.

also reported in figure 9. As can be seen, they represent an intermediate set among the various experimental data and are really in good agreement with the sets recently published by Andreozzi *et al* [4] and Maekawa *et al* [7]. This confirms the ability of infrared spectroscopy, and more especially emittance measurements, to provide an *in situ* estimation of the inversion parameter over a very wide range of temperature.

Another thermodynamic approach proposed by O'Neill and Navrotsky [35] is often used to reproduce the temperature dependence of the inversion parameter. The model predicts a

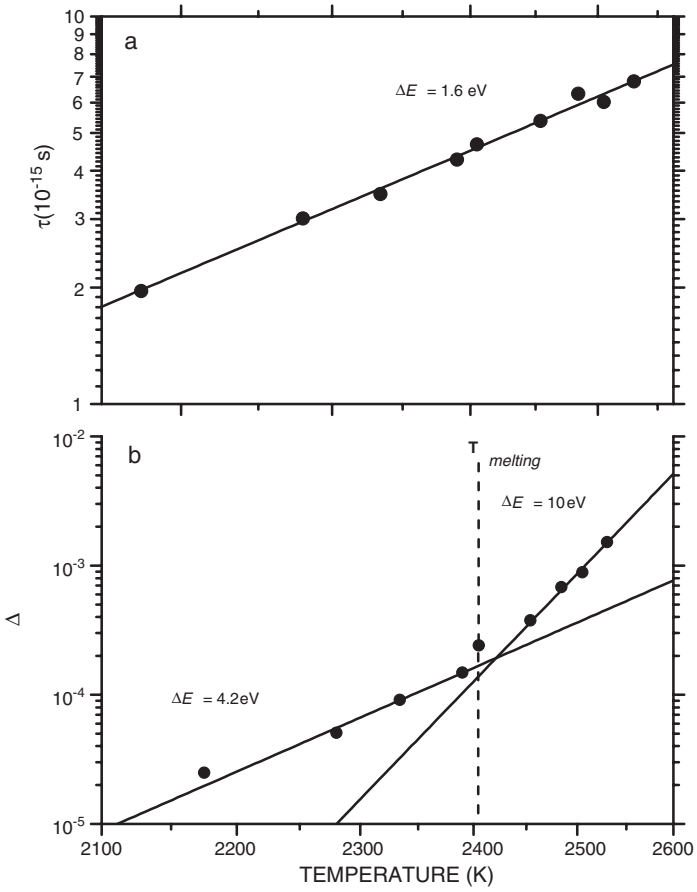

Figure 12. Temperature dependence of the dielectric contribution Δ and of the characteristic time τ of the Debye relaxation. Lines represent least square fits of the experimental data using an Arrhenius model and ΔE the corresponding activation energies.

temperature dependence of the inversion parameter x that is given by the following relation:

$$T = \frac{\alpha + 2\beta x}{R} \ln\left(\frac{(1-x)(2-x)}{x^2}\right), \tag{22}$$

where R is the ideal gas constant and α, β are the free adjustable parameters. The best fit of $x_{4\&6}$ using equation (22) is obtained for the values $\alpha = 24$ kJ mol^{-1} and $\beta = 16$ kJ mol^{-1}, which are very close to those reported by Andreozzi *et al* [4]. Figure 9 shows that both the Landau and the O'Neill and Navrotsky models lead to adjustments of similar quality, so further work is needed to make a choice between the two types of model.

5. Solid to liquid transition

In the second set of measurements, we used the autocrucible technique to investigate the solid to liquid transition occurring around 2400 K. A representative set of emittance spectra and their best fits are reported in figure 10 and the corresponding temperature dependences of the absorption coefficient are shown in figure 11. The figures show a rapid increase in the emittance

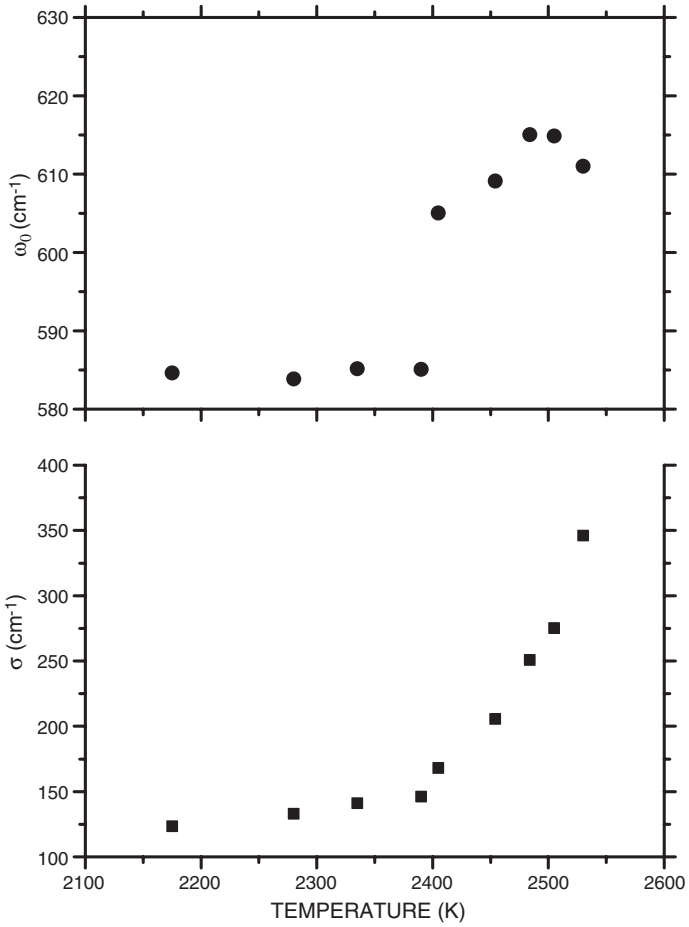

Figure 13. Effect of the solid to liquid phase transition on frequency and full width at half maximum of the ν_8 mode of $MgAl_2O_4$.

in the mid-infrared range (i.e. above 3000 cm^{-1}), more than 200 degrees below the appearance of the liquid state. Similar behaviour was also seen in other materials such as MgO or Al_2O_3 but not in silica [28]. Its spectral dependence is well described by the addition of a Debye term in the dielectric function. Least square fits of the experimental data show that the relaxational process is thermally activated. The activation energy of the dielectric contribution Δ changes from about 4.2 eV in the solid state to 10 eV in the liquid state (figure 12). The relaxation time τ is also thermally activated (1.6 eV) but in this case no modification of the activation energy is seen at the phase transition. *The very small characteristic time of the relaxation suggest that this absorption is an electronic contribution.*

Other important modifications occur in the phonon zone, but due to the limited spectral range of this second set of measurements, only results concerning the highest frequency mode are reported. Figure 13 shows that at the solid to liquid transition the phonon frequency undergoes a drastic increase. The full width at half maximum of the mode also increases rapidly in the liquid phase. This behaviour is consistent with the sudden structural change that occurs at the transformation. Changes in the liquid state are also characteristic of a rapid evolution

of dynamics in this phase. No link can be proposed between the observed disorder and the description of the thermally activated behaviour more than 200 K before the melting point.

6. Conclusion

The unique experimental results combined with adequate tools for spectral analysis allowed us to characterize the lattice dynamics of $MgAl_2O_4$ up to the liquid state and to retrieve the inversion parameter over a very wide range of temperature. Landau functions and the O'Neill and Navrotsky thermodynamic model have been successfully used to fit the experimental data with values for the latter that are very close to those reported recently by Andreozzi *et al* [4]. Even if no definitive conclusion can be made on the most adequate thermodynamic model, these results confirm that infrared emission spectroscopy can be used to make *in situ* evaluations of the cation disorder in such types of material. In the same way, infrared spectroscopy is very sensitive to the onset of absorption mechanisms in the high temperature domain. Like some other dielectric oxides, in the mid-infrared range $MgAl_2O_4$ exhibits a sudden increase of emittance more than 200 degrees below the solid to liquid transition. The mechanism of absorption is very well described by a Debye process where both its dielectric contribution and relaxation time are thermally activated. Finally, we showed that the change of phase leads to an abrupt modification of the lattice dynamics and that change evolves rapidly in the liquid state. The two high temperature features revealed in this paper seem to be unrelated.

References

[1] Wang Q, Cheng J and Wu S 2002 *Japan. J. Appl. Phys.* **41** 61110
[2] Afanasyev-Charkin I V, Cooke D W, Ishimaru M, Bennett B L, Gritsyna V T, Williams J R and Sickafus K E 2001 *Opt. Mater.* **16** 397
[3] Smith R, Bacorisen D, Uberuaga B P, Sickafus K E, Ball J A and Grimes R W 2005 *J. Phys.: Condens. Matter* **17** 875
[4] Andreozzi G B, Princivalle F, Skogby H and Della Giusta A 2000 *Am. Mineral.* **85** 1164
[5] Redfern S A T, Harrisson R J, O'Neill H S C and Wood D R R 1999 *Am. Mineral.* **84** 299
[6] Andreozzi G B and Princivalle F 2002 *Am. Mineral.* **87** 838
[7] Maekawa H, Sato S, Kawamura K and Yokokawa T 1997 *Am. Mineral.* **82** 1125
[8] Millard R L, Peterson R C and Hunter B K 1992 *Am. Mineral.* **77** 44
[9] Peterson R C, Lager C A and Hitterman R L 1991 *Am. Mineral.* **76** 1455
[10] Wood B J, Kirkpatrick R J and Montez B 1986 *Am. Mineral.* **71** 999
[11] Méducin F, Redfern S A T, Le Godec Y, Stone H J, Tucker M G, Dove M T and Marshall W G 2004 *Am. Mineral.* **89** 981
[12] Harrison R J, Dove M T, Knight K S and Putnis A 1999 *Am. Mineral.* **84** 555
[13] Da Rocha S and Thibaudeau P 2003 *J. Phys.: Condens. Matter* **15** 7103
[14] Warren M C, Dove M T and Redfern S A T 2000 *Mineral. Mag.* **64** 311
[15] Warren M C, Dove M T and Redfern S A T 2000 *J. Phys.: Condens. Matter* **12** L43
[16] Warren M C, Dove M T, Myers E R, Bosenick A, Palin E J, Sainz-Diaz C I, Guiton B S and Redfern S A T 2001 *Mineral. Mag.* **65** 221
[17] Slack G A 1964 *Phys. Rev.* **134** A1268
[18] Preudhomme J and Tarte P 1971 *Spectrochim. Acta* A **27** 1817
[19] Boguslavska N N, Venger E F, Vernidub N M, Pasechnik Y A and Shportko K V 2002 *Semicond. Phys. Quantum Electron. Optoelectron.* **5** 95
[20] Chihara H, Tsuchiyama A, Koike C and Sogawa H 2000 *Disks, Planetesimals and Planets* (*ASP Conf. Series* vol 219) ed F Garzón, C Eiroa, D de Winter and T J Mahoney (San Francisco: Astronomical Society of the Pacific) p 150
[21] Posch T, Kerschbaum F, Mutschke H, Fabian D, Dorschner J and Hron J 1999 *Astron. Astrophys.* **352** 609
[22] Fabian D, Posch T, Mutschke H, Kerschbaum F and Dorschner J 2001 *Astron. Astrophys.* **373** 1125
[23] Thibaudeau P and Gervais F 2002 *J. Phys.: Condens. Matter* **14** 3543
[24] Cynn H, Sharma S K, Cooney T F and Nicol M 1992 *Phys. Rev.* B **45** R500

[25] Minh N V and Yang I 2004 *Vibr. Spectrosc.* **35** 93
[26] Lauwers H A and Herman M A 1980 *J. Phys. Chem. Solids* **41** 223
[27] de Wijs G A, Fang C M, Kresse G and de With G 2002 *Phys. Rev.* B **65** 094305
[28] Rozenbaum O, De Sousa Meneses D, Auger Y, Chermanne S and Echegut P 1999 *Rev. Sci. Instrum.* **70** 4025
[29] De Sousa Meneses D, Brun J F, Echegut P and Simon P 2004 *Appl. Spectrosc.* **58** 969
[30] De Sousa Meneses D, Gruener G, Malki M and Echegut P 2005 *J. Non-Cryst. Solids* **351** 124
[31] Focus Web Site http://crmht.cnrs-orleans.fr/pot/software/focus.html
[32] Tropf W J, Thomas M E and Haris T J 1995 Properties of crystals and glasses *Handbook of Optics, Devises, Measurements and Properties* 2nd edn, vol 2, ed M Bass, E W Van Stryland, D R Williams and W L Wolfe (New York: McGraw-Hill) chapter 33
[33] Carpenter M A and Salje E K H 1994 *Am. Mineral.* **79** 1068
[34] Carpenter M A, Powell R A and Salje E K H 1994 *Am. Mineral.* **79** 1053
[35] O'Neill H St C and Navrotsky A 1983 *Am. Mineral.* **68** 181